International Journal of Minerals, Metallurgy and Materials
Volume 24, Number 12, December 2017, Page 1384
DOI: 10.1007/s12613-017-1531-1

Effect of weld line positions on the tensile deformation of two-component metal injection moulding

Anchalee Manonukul[1)], *Sukrit Songkuea*[1)], *Pongporn Moonchaleanporn*[1)], *and Makiko Tange*[2)]

1) National Metal and Materials Technology Center (MTEC), National Science and Technology Development Agency (NSTDA), 114 Thailand Science Park, Paholyothin Road, Klong 1, Klong Luang, Pathumthani 12120, Thailand

2) Taisei Kogyo (Thailand) Co., Ltd., Room INC2D-409, Innovation Cluster 2 Building, Tower D, 141 Thailand Science Park, Paholyothin Road, Klong 1, Klong Luang, Pathumthani 12120, Thailand

(Received: 13 March 2017; revised: 19 May 2017; accepted: 22 May 2017)

Abstract: Knowledge of the mechanical properties of two-component parts is critical for engineering functionally graded components. In this study, mono- and two-component tensile test specimens were metal injection moulded. Three different weld line positions were generated in the two-component specimens. Linear shrinkage of the two-component specimens was greater than that of the mono-component specimens because the incompatibility of sintering shrinkage of both materials causes biaxial stresses and enhances sintering. The mechanical properties of 316L stainless steel were affected by the addition of a coloured pigment used to identify the weld line position after injection moulding. For the two-component specimens, the yield stress and ultimate tensile stress were similar to those of 316L stainless steel. Because 316L and 630 (also known as 17-4PH) stainless steels were well-sintered at the interface, the mechanical properties of the weaker material (316L stainless steel) were dominant. However, the elongations of the two-component specimens were lower than those of the mono-component specimens. An interfacial zone with a microstructure that differed from those of the mono-material specimens was observed; its different microstructure was attributed to the gradual diffusion of nickel and copper.

Keywords: co-meal injection moulding; 316L stainless steel; 630 stainless steel; joining position; tensile deformation

1. Introduction

Two-component metal structures as functionally graded components offer performance advantages over individual materials. An example is wear-resistant tool steel (T15, M2, or D2) inserted with high-toughness-resistant metals (boron-doped 316L stainless steel, Fe–2Ni, 4340, or Fe–10Cr) [1]. A suitable pair of metals should have good metallurgical bonding and similar sintering shrinkage throughout the sintering process to avoid the occurrence of defects such as cracks and delamination. Heaney *et al.* [1] have suggested that the M2 and 316L–0.5B combination is the most suitable. Another example is a component surface of 316L stainless steel surrounding a core of carbonyl iron for high corrosion resistance on the surface [2]. Other case studies include non-magnetic and magnetic materials, e.g. a magnetic positioning encoder consisting of a 316L stainless steel non-magnetic bar with two 630 (also known as 17-4PH) stainless steel ferromagnetic ends, and a tachometer with a non-magnetic 316L stainless steel body and one ferromagnetic 630 stainless steel wing [3]. Two-component metal parts can also be used as heat sinks with controlled porosity and high thermal conductivity. One example is a solid copper body with cooling fins, surrounding a porous wick, which serves as a heat pipe [4].

Two-component parts have traditionally been fabricated by several techniques, e.g. welding, brazing, or soldering. However, these traditional fabrication methods introduce a third material as a filler or adhesive, which can substantially change the properties of two-component parts, especially the electrical properties, and also become a weak point. Two-component metal injection moulding (2C-MIM) or metal co-injection moulding has been used as an alternative fabrication method to produce two-component parts with

Corresponding author: Anchalee Manonukul E-mail: anchalm@mtec.or.th

highly complex geometries. The injection moulding step in 2C-MIM is similar to plastic two-component injection moulding. However, the co-debinding and co-sintering steps are the main challenge in 2C-MIM. Therefore, previous works involving 2C-MIM were focused on achieving a good co-sintering interface between the two materials without any interfacial cracks by minimising the differences in shrinkage [5]. Furthermore, not only the difference in shrinkage at the end of sintering but also the difference in shrinkage throughout the sintering cycle must be carefully controlled and minimised. The authors of previous studies have reported good interfacial bonding between 316L/630 stainless steels [6]. Microstructural observations using optical microscopy (OM) and scanning electron microscopy (SEM) were used to identify the interface [7]. The diffusion of nickel from 316L stainless steel into 630 stainless steel was also observed using energy-dispersive X-ray spectroscopy (EDS) analysis [7]. The width of the diffusion zone was relatively narrow—on the order of 50 μm; however, this diffusion zone was not observed in any micrographs [3].

Because two-component parts can be used as structural engineering components, their corresponding mechanical properties are highly important. However, the literature contains few published works focused on the mechanical properties of such components. Imgrund *et al*. [3] reported that the ultimate tensile strengths of microinjection-moulded mono-component 316L stainless steel and 630 stainless steel and two-component 316L/630 stainless steel are 450, 800, and 670 MPa, respectively, but provided no further details. Microinjection-moulded mono-component 430 stainless steel and 314 stainless steel and two-component 430/314 stainless steel have also been studied [8]. All tensile samples of the 430 stainless steel, which was the weakest material among those studied, failed. The tensile strength of the two-component 430/314 stainless steel was comparable to the strength of the mono-component 630 stainless steel. Joining of 316L stainless steel and 430L stainless steel using insert injection moulding has also been investigated [9]. The joining strength of 316L/430L stainless steel was lower than that of the same materials, i.e. 316L/316L stainless steel or 430L/430L stainless steel, in the studied sintering temperature range from 1100 to 1350°C.

Several techniques for polymer co-injection moulding have been developed. Two-component parts can be sequentially moulded or simultaneously moulded. The mechanical properties of polymer two-component tensile test specimens have been reported to noticeably differ [10]. In addition, for simultaneous moulding, the weld line can be altered using different injection parameters, which can, in turn, affect the mechanical properties of polymer co-injection moulding specimens [11]. Therefore, the objective of this work is to systematically and experimentally investigate the effects of weld line position on the mechanical and physical properties of two-component 316L/630 stainless steel. Two-component tensile specimens with three different weld line positions were investigated. In addition, the mono-component 316L stainless steel and 630 stainless steel were characterised for comparison.

2. Experimental

2.1. Preparation of two-component metal injection moulding specimens

Feedstocks for 2C-MIM consist of either water-atomised 316L or 630 (17-4PH) stainless steel powders and a polyacetal-based binder. Table 1 shows the chemical compositions of 316L and 630 (17-4PH) stainless steel powders and the corresponding Metal Powder Industries Federation (MPIF) standard 35 [12]. The chemical compositions of both stainless steel powders conformed to the MPIF standard. The stainless steel powders, which were supplied by Epson Atmix Corporation, Japan, were rounded, with minimal satellite particles. The average powder sizes (D_{50}) were 10.86 μm for the 316L stainless steel powder and 9.77 μm for the 630 stainless steel powder. The binder was supplied by Mould Research Co., Ltd., Japan and was designed for a single 24-h thermal cycle of debinding and sintering to save processing time. Mono-component 316L stainless steel and 630 stainless steel feedstocks were mixed using mixing ratios of 62:38 and 60:40 by volume of metal powder and binder respectively. To identify the weld line positions and help distinguish the two materials during the "green" stage (after injection moulding, before debinding and sintering), 1.96wt% (8.82vol%) of pink-coloured pigment was added to the 316L stainless steel feedstock. Hence, the effective solid loading in the 316L stainless steel feedstock containing pink-coloured pigment was 56.53% by volume. The pink-coloured pigment was supplied by PolyOne (Thailand) Co., Ltd., Thailand (catalog no. 6Y16940). Subsequently, mono-component 316L stainless steel and 630 stainless steel feedstocks were mono- and co-injection moulded into the tensile test specimen shapes using a Nissei DCE60-2E horizontal co-injection moulding machine. The injection temperatures were 175°C for 316L stainless steel and 180°C for 630 stainless steel. Injection unit A was used to inject the 316L stainless steel feedstock, whereas injection unit B was used for the 630 stainless steel feedstock. Most parameters were kept constant for both injection units. The shot size was 20 mm. The injection pressure was 150 MPa. The ve-

locity–pressure (v–P) position was 7 mm. The limited velocity was 20 mm·s^{-1}, and the holding pressure was 50 MPa. To obtain samples with different weld-line positions, the injection velocity was varied as shown in Table 2. For the weld lines to meet at the centre, the injection velocity of both injection units were set to 20 mm·s^{-1}. Notably, the weld line was not exactly in the middle, suggesting that the viscosities of the two feedstocks were not exactly the same. Although the same binder was used, a difference in viscosity was possible because metal powders and mixing ratios differed; in addition, pink-colour pigment was added in the 316L stainless steel feedstock.

Table 1. Chemical compositions of 316L stainless steel and 630 stainless steel powders and the corresponding MPIF standard 35 [12] wt%

Powder	C	Si	Mn	P	S	Ni	Cr	Mo	Cu	O / ppm	Nb + Ta
316L	0.024	0.81	0.80	0.019	0.009	12.53	16.49	2.10	0.03	3400	—
MPIF 316L	0.03 (max)	1.0 (max)	2.0 (max)	—	—	10–14	16–18	2–3	—	—	—
630	0.051	0.81	0.78	0.023	0.006	4.24	15.69	0.01	3.23	3500	0.30
MPIF 630	0.070 (max)	1.0 (max)	1.0 (max)	—	0.03 (max)	3–5	15.5–17.5	—	3–5	—	0.15–0.45

Table 2. Injection velocity of preparing mono- and two-component tensile test specimens to obtain different weld line positions

Sample	Injection velocity / (mm·s^{-1})	
	Injection unit A (316L)	Injection unit B (630)
316L	27	15
14.5% 630*	22	20
56.6% 630*	20	20
86.4% 630*	20	22
630	15	27

Note: * — These samples are two-component tensile test specimens with various weld line positions, i.e., with different average percentages of 630 stainless steel within the gauge length, for example, in "14.5% 630" sample, the average percentage of 630 stainless steel within the gauge length is 14.5%, whereas that of 316L is 85.5%.

To have more portion of 316L stainless steel within the gauge length, the injection speed of injection unit A (316L) was increased slightly to 22 mm·s^{-1} while the injection speed of injection unit B (630) was kept constant. When the injection speed of injection unit A (316L) was increased to 27 mm·s^{-1} and that of injection unit B (630) was decreased to 15 mm·s^{-1}, the entire tensile sample was 316L stainless steel. The weld line position was in the runner nearly to injection unit B (630). To achieve a greater portion of 630 stainless steel, the injection velocity of injection unit B (630) was set higher than that of injection unit A (316L). Two sets of mono-component specimens and three sets of two-component specimens with three different weld line positions were produced, as shown in Fig. 1 (top row). The five green specimens in Fig. 1 are mono-component 316L stainless steel (left), mono-component 630 stainless steel (right), and three two-component 316L/630 stainless steels (middle). A portion of the specimens that contains 630 stainless steel is grey, and a portion of the 316L stainless steel specimens are pinkish grey. The green parts were thermally debonded at 450°C for 1 h to remove the binder and then sintered at 1350°C for 2 h under an argon atmosphere.

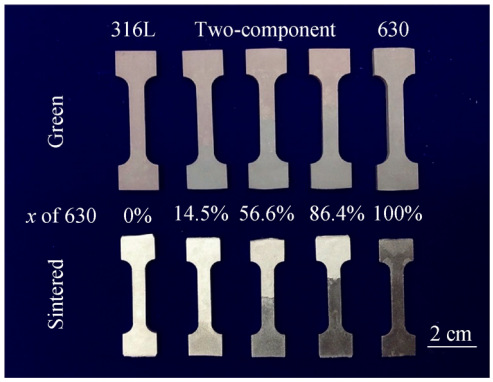

Fig. 1. Green and sintered mono- and two-component tensile test specimens showing various weld line positions and different average percentages of 630 stainless steel within the gauge length (x).

2.2. Analysis

The average sintered density was measured using the water immersion method according to MPIF standard 42 [13]. In addition, the microstructures were examined using three-dimensional optical microscopy (3D-OM) and scanning electron microscopy (SEM). For SEM analysis, the acceleration voltage was 20 kV, the working distance was 10 mm, and the emission current was 50–70 μA. The two-component specimens were etched by the following method: when one material was etched, the other material was coated with vaseline. Chemical compositions were also analysed using X-ray dif-

fraction (XRD) and SEM/EDS. The analysis parameters for XRD were 50 kV and 300 mA. The tensile tests were carried out at room temperature and at a constant rate of 0.13 mm·min^{-1} using a 25-kN universal testing machine. The tensile tests were repeated three times for each set of experiments.

The weld line position was quantified using the average percentage of 630 stainless steel within the gauge length (x), as shown in Eq. (1):

$$x = \frac{L_{630}}{L_g} \times 100\% \quad (1)$$

where L_g and L_{630} are the gauge length distance and the distance of 630 stainless steel within the gauge length, respectively, as shown in Fig. 2. Therefore, the 316L stainless steel specimens had x = 0% and the 630 stainless steel specimens had x = 100%. The three two-component 316L/630 stainless steel specimens had x = 14.5%, 56.6%, and 86.4% respectively, as shown in Fig. 1. Notably, these values for the average percentage of 630 stainless steel within the gauge length (x) were based on the measurements of sintered specimens (bottom row in Fig. 1).

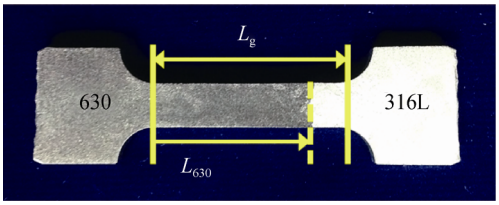

Fig. 2. Sintered two-component tensile test specimen showing the gauge length distance and the distance of 630 stainless steel within the gauge length.

3. Results and discussion

3.1. Density and shrinkage

Fig. 1 shows a photograph of green and sintered mono- and two-component tensile test specimens. In the case of the green parts, the weld line and the difference in grade of stainless steel are distinguished by the pink-coloured pigment added to the 316L stainless steel feedstock. In the case of the sintered parts, both stainless steels exhibit a metallic colour with different levels of glossiness; the weld-line position is identified as shown in Fig. 2. Fig. 3 shows the average green and sintered densities of the mono- and two-component tensile test specimens in Fig. 1 as a function of the average percentage of 630 stainless steel within the gauge length (x). The green density of the 316L stainless steel specimens (x = 0%) was slightly lower (0.06 g·cm^{-3}) than that of the 630 stainless steel specimens (x = 100%), mainly because of the addition of 1.96wt% pink-coloured pigment, despite the higher theoretical density of 316L stainless steel compared to that of 630 stainless steel. The green density of the two-component specimens was intermediate between the densities of the mono-component 316L stainless steel and the mono-component 630 stainless steel specimens.

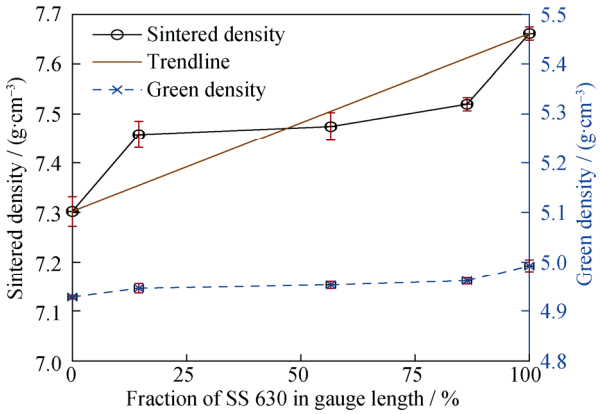

Fig. 3. Average green and sintered densities of mono- and two-component tensile test specimens as a function of the average percentage of 630 stainless steel within the gauge length (SS represents stainless steel).

After sintering, densities of all of the specimens increased, on average, by 2.5 g·cm^{-3}, as shown in Fig. 3. The variation in sintered density shows a trend similar to that of the green density. The relative density of 630 stainless steel specimens (x = 100%) is 97.5%, which is typical for well-sintered metal injection moulded parts. However, the relative density of the 316L stainless steel is only 92.9%, which is substantially lower than that of standard metal injection moulded parts. This discrepancy suggests that the introduction of the coloured pigment hinders the sintering of 316L stainless steel. The sintered density calculated for the measured densities of mono-component 316L stainless steel and mono-component 630 stainless steel specimens on the basis of the rule of mixture is also shown as a straight line linking the two densities. Notably, the rule of mixture was only applicable for specimens with a constant cross section. However, the tensile specimens in this work, as shown in Fig. 2, had a constant cross section within the gauge length and a larger cross-sectional area in the gripping areas. The calculated sintered density line intercepts the measured sintered density line at x = 50%, where the specimen is symmetrical and where the effect of a non-constant cross section is eliminated. In cases where the length of 630 stainless steel within the gauge length is less than 50% (x < 50%), the predicted rule-of-mixture density of the two-component specimen should be less than the measured density. However, in cases

where the 630 stainless steel length within the gauge length is greater than 50% (x > 50%), the predicted rule-of-mixture density of the two-component specimen should be greater than the measured density. These predictions agree well with the experimental results, as shown in Fig. 3. In addition, the sintered density of two-component specimens linearly increases with increasing percentage of 630 stainless steel within the gauge length.

Fig. 4 shows the average linear shrinkage of mono- and two-component tensile test specimens in Fig. 1 as a function of the average percentage of 630 stainless steel within the gauge length (x). To eliminate the effect of the non-constant cross section, the linear shrinkage should be the shrinkage of the gauge length (L_g), as shown in Fig. 2. A comparison of the linear shrinkage of the mono-component specimens revealed that 316L stainless steel exhibited a slightly lower linear shrinkage than 630 stainless steel. This result is consistent with the lower relative density of 316L stainless steel and with the slightly higher solid loading of the feedstock. The linear shrinkage of the two-component specimens increased with increasing percentage of 630 stainless steel within the gauge length. Notably, however, the shrinkages of both of the mono-component specimens were lower than those of the two-component specimens, as evident in Fig. 1. This result suggests that the two materials interacted at the interface and caused greater shrinkage than that exhibited by either of the mono-component materials. Densification of the composite layer of 316L/630 stainless steel has been reported to be enhanced during co-sintering [7]. Enhanced densification has also been observed in the co-sintering of M2/316L [14] and at the interface of M2/630 [15]. Firouzdor *et al.* [14–15] suggested that this enhanced densification is caused by sintering-shrinkage incompatibility between two materials and the interlayer diffusion of alloying elements and by the formation of a dual δ-ferrite/austenite phase at high temperatures. Sintering incompatibility between two materials develops biaxial stresses in the interfacial areas and enhances the sintering kinetics [16].

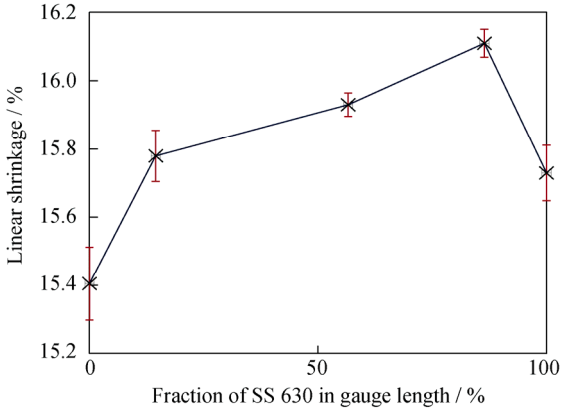

Fig. 4. Average linear shrinkage of mono- and two-component tensile test specimens as a function of the average percentage of 630 stainless steel within the gauge length (SS represents stainless steel).

3.2. Mechanical properties

Fig. 5 shows the representative tensile responses of sintered mono- and two-component specimens. In addition, Fig. 6 shows the corresponding average yield strength, ultimate tensile strength, and elongation at break. The mono-component 630 stainless steel samples (x = 100%) exhibited typical ductile behaviour, with large elongation after the ultimate tensile stress was reached. The corresponding average yield strength, ultimate tensile strength, and elongation at break were 445 MPa, 896 MPa, and 9.9%, respectively. The measured ultimate tensile strength (896 MPa) and elongation at break (9.9%) are well above the minimum values stated in MPIF standard 35 (790 MPa and 4%), and the ultimate tensile strength (896 MPa) agrees well with the typical value (900 MPa) stated in MPIF standard 35 [12]. The typical value for the elongation at break of MPIF 630 stainless steel is 6.0%; the sintered elongation measured in the present work (9.9%) is well above this value. The large elongation after the ultimate tensile strength was also evidenced as necking in fracture samples, as shown in Fig. 7 (x = 100%).

For mono-component 316L stainless steel specimens (x = 0%), the ductile tensile response showed small elongation after reaching the ultimate tensile strength and the average elongation was 10.2%. Minimal necking is observed in Fig. 7 (x = 0%); this behavior is extremely unusual for 316L stainless steel, which should exhibit a minimum elongation of 40% and a typical elongation of 50% according to MPIF

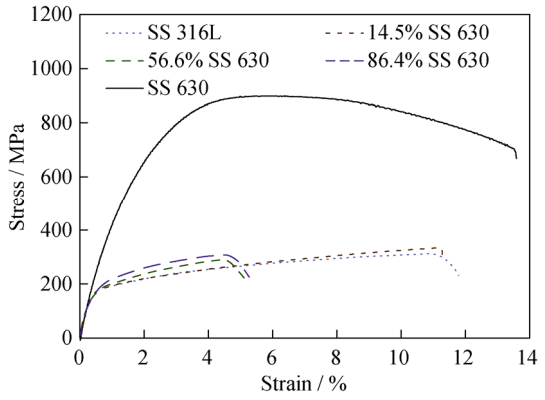

Fig. 5. Representative tensile results for sintered mono- and two-component tensile test specimens (SS represents stainless steel).

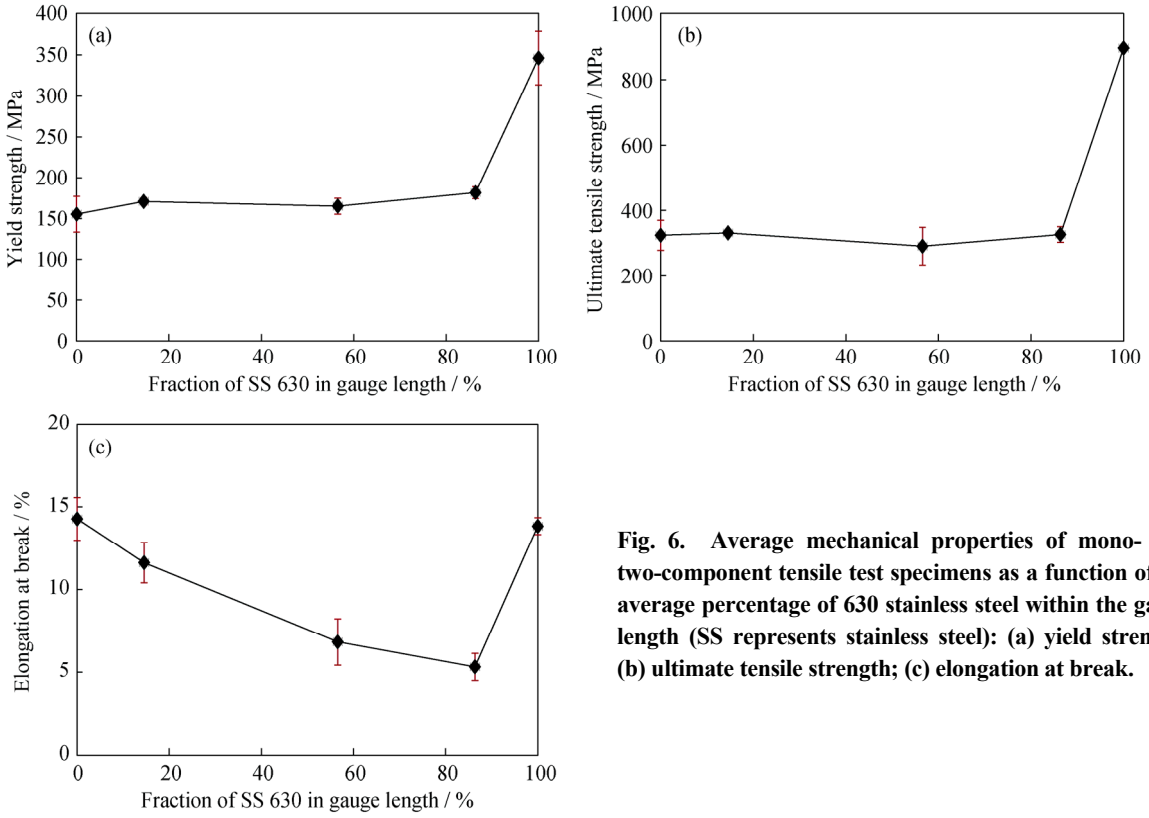

Fig. 6. Average mechanical properties of mono- and two-component tensile test specimens as a function of the average percentage of 630 stainless steel within the gauge length (SS represents stainless steel): (a) yield strength; (b) ultimate tensile strength; (c) elongation at break.

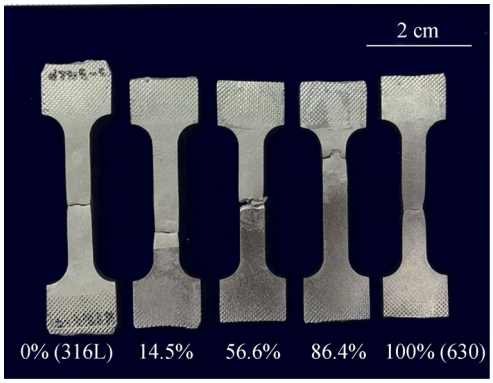

Fig. 7. Fractured mono- and two-component tensile test specimens.

standard 35 [12]. In addition, the ultimate tensile strength was 324 MPa, which is also well below the minimum MPIF ultimate tensile strength of 450 MPa. The significant reduction in elongation and ultimate tensile strength is likely due to the addition of the coloured pigment, which reduced the sintered relative density to less than 93%. Notably, the 316L stainless steel was also metal injection moulded without the pigment. In this case, an as-sintered relative density of 97.5% was achieved and the tensile properties well satisfied MPIF standard 35 [12], with 49% elongation. The addition of the coloured pigment substantially reduced the powder loading from 62% to 56.53%, which adversely reduced the tensile properties of 316L stainless steel.

For two-component specimens, the tensile responses showed small elongation after reaching the ultimate tensile strength, similar to the mono-component 316L stainless steel specimens (x = 0%). Minimal necking is also evident in Fig. 7 (x = 14.5%, 56.6%, and 86.4%), similar to the behaviour of the mono-component 316L stainless steel specimens. Fracture occurred near the interface of the two materials but always on the 316L stainless steel portion. This behaviour indicates that the *in-situ* strength of 316L stainless steel was lower than that of 630 stainless steel and lower than the interfacial strength [17]. In addition, the 316L and 630 stainless steels were compatible, resulting in good bonding. This good bonding is evident from the mono-component tensile results, which show that the 630 stainless steel exhibited substantially greater strength than the 316L stainless steel and that fracture did not occur at the interface. As the percentage of 630 stainless steel within the gauge length was increased, the average elongation at break decreased for the two-component specimens. This result is also in good agreement with the photograph of fracture tensile specimens shown in Fig. 7.

As shown in Fig. 6, the average yield and ultimate tensile strengths of the two-component specimens (x = 14.5%, 56.6%, and 86.4%) were similar to those of the mono-component 316L stainless steel specimens (x = 0%).

This similarity suggests that the weaker material in the two-component specimen dictates the strength of the two-component material specimen if the two materials are compatible and that the strength is independent of the percentage of 630 stainless steel within the gauge length.

3.3. Microstructure and chemical analysis

Fig. 8 shows the as-polished micrographs of the sintered interface between 316L and 630 stainless steels using two different magnifications. The dashed line indicates the weld line between the two materials, where the upper portion is 630 stainless steel and the lower portion is 316L stainless steel. The black frame in Fig. 8(a) indicates the location of Fig. 8(b). The weld line was not perfectly straight because a simultaneous co-injection moulding process was used. Two materials were injected from two nozzles into the opposite ends of a tensile test specimen and then flowed to join each other. No cracking or warpage was observed at the interface. This result is in good agreement with the mechanical property results that indicated the two materials were compatible and that both materials were bonded soundly. Some small rounded residual pores were observed because the sample was subjected to pressureless sintering. In the case of the 630 stainless steel, the trace of grain structure was observed at the as-polished stage; no such structure was observed for the 316L stainless steel.

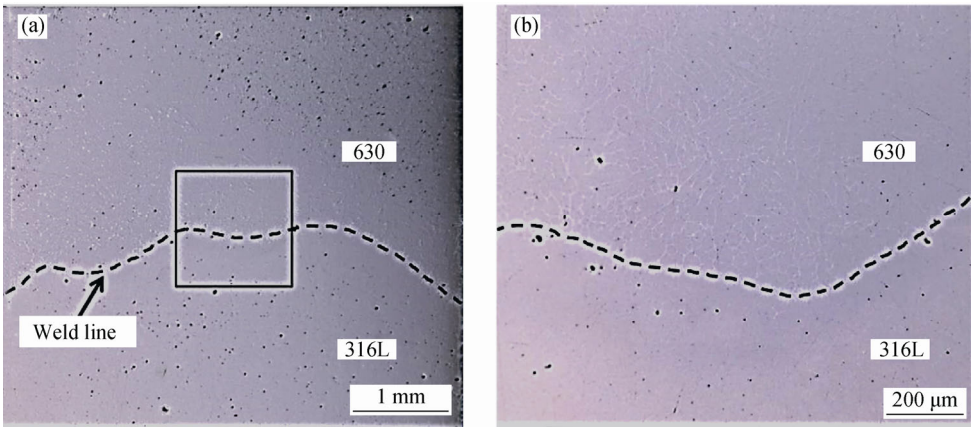

Fig. 8. As-polished micrographs of the sintered interface between two materials at different magnifications (the black frame in (a) shows the location of (b)).

Fig. 9 shows the etched micrographs of the sintered interface between the 630 and the 316L stainless steels at three different magnifications. Instead of only two different microstructural zones previously reported for co-sintered 316L/630 stainless steel [7], three different zones of microstructures were observed in this work. Away from the interfacial zone, the 630 stainless steel exhibited martensitic elongated laminar grains with islands of ferrite at the grain boundaries, whereas the 316L stainless steel exhibited equiaxed austenitic grains, as typically observed in sintered samples of both materials [18]. However, an interfacial zone was observed, where the microstructure was neither 316L stainless steel nor 630 stainless steel. This zone was easily etched, similar to 630 stainless steel; however, the microstructure was not elongated. The microstructure in this interfacial zone contained a band of slightly greater porosity near the 316L interface. This greater porosity was due to the Kirkendall effect, which has also been observed in the interface of M2/316L samples [14] and in the interface of M2/630 samples [15] co-sintered at a relatively high sintering temperature of 1290°C for 90 min under a mixed Ar/H_2 atmosphere. Notably, a porosity band was not observed at lower sintering temperatures [14–15]. In the present work, the samples were sintered at 1350°C for 2 h under argon and a porosity band was observed. Notably, the interfacial zone was not observed in the as-polished samples (Fig. 8).

The contents of nickel and copper are the main difference between 316L and 630 stainless steels. In the present work, the 316L stainless steel powder contained 12.53wt% nickel and 0.03wt% copper, whereas the 630 stainless steel powder contained 4.24wt% nickel and 3.23wt% copper, as shown in Table 1. These differences in alloying element contents resulted in different microstructures. Fig. 10 shows theSEM micrographs and EDS line analysis results for the interfacial zone. The left portion is 316L stainless steel, and the right portion is 630 stainless steel. The SEM micrograph shows more porosities at the interfacial zone. The 316L stainless steel contains more nickel but less copper than the 630 stainless steel, as expected. In the interfacial zone, nickel gradually diffused from the 316L stainless steel toward the 630 stainless steel and copper gradually diffused from the 630 stainless steel toward the 316L stainless steel. The

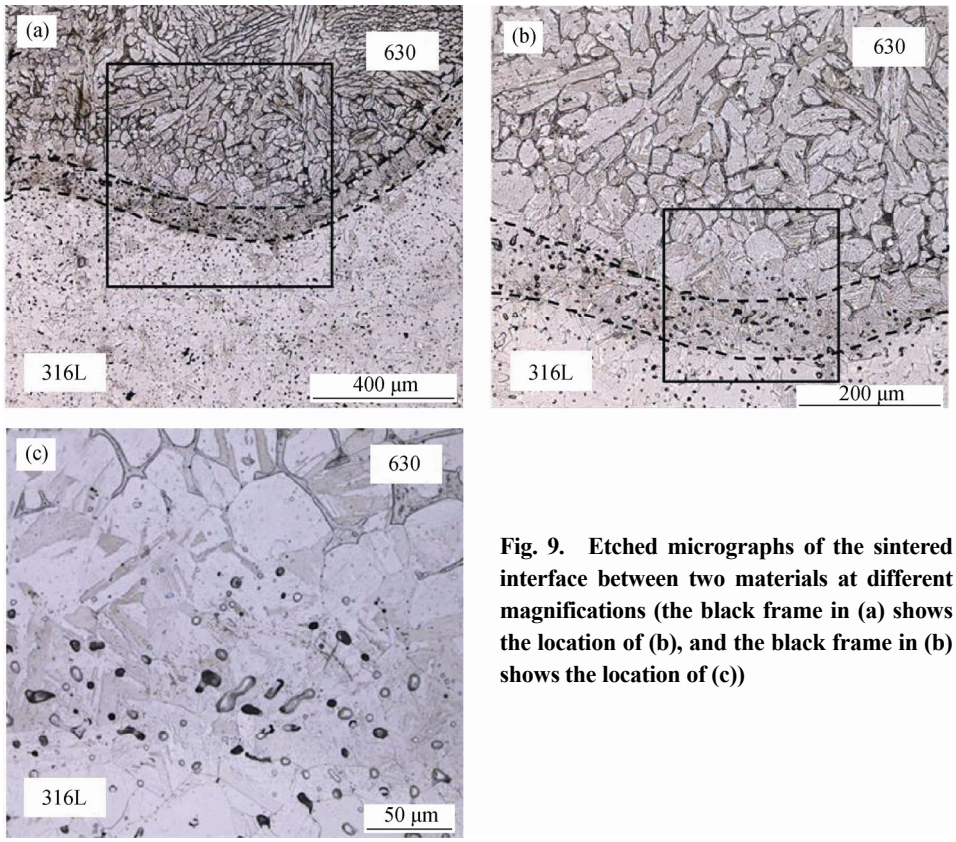

Fig. 9. Etched micrographs of the sintered interface between two materials at different magnifications (the black frame in (a) shows the location of (b), and the black frame in (b) shows the location of (c))

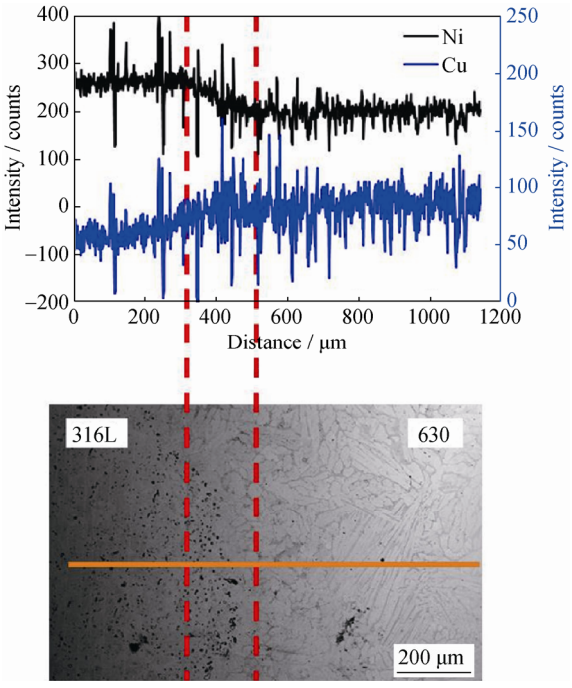

Fig. 10. SEM/EDS analysis of the sintered interface between 316L and 630 stainless steels.

interfacial zone was approximately 180 μm, which is three times larger than the narrow "diffusion" zone reported elsewhere [3] for a sample sintered at 1300°C for 1 h under hydrogen. Notably, in the present work, the samples were sintered at 1350°C for 2 h under argon. Therefore, these results suggest that the width of the interfacial zone increased with both increasing sintering temperature and increasing sintering time. In a previous study of 2C-MIM of 430 and 314 stainless steels, this interfacial zone was identified as a dual-phase ferritic–austenitic diffusion layer [14].

Fig. 11 shows the typical micrographs of the fracture surfaces for mono-component 316L stainless steel (x = 0%), two-component (x = 56.6%), and mono-component 630 stainless steel (x = 100%) tensile test specimens. The fracture surfaces of all three sets of two-component specimens are similar; hence, only x = 56.6% is shown. All of the fracture surfaces show dimples associated with ductile failure, in good agreement with the elongation shown in Figs. 5 and 6 and with necking observed in Fig. 7. The fracture surfaces of the 316L stainless steel and the two-component specimens were similar, as indicated by the fracture of the two-component specimens occurring in the 316L stainless steel portion near the interface on the 316L stainless steel side, as shown in Fig. 7. The sizes of dimples varied; however, in general, the dimple sizes of 316L stainless steel and the two-component samples were larger than those of 630 stainless steel. In the case of the fracture surface of the 630 stainless steel shown in Fig. 11(c), islands

of ferrite surrounded by dimples were also observed. A similar fracture surface for 630 stainless steel has been reported elsewhere [19].

Fig. 12 shows the XRD analysis results for the sintered 316L stainless steel with the added pigment and for 630 and 316L stainless steels without the pigment. The results for the 316L stainless steel without the pigment are included for reference to demonstrate the effect of pigment addition. The XRD pattern of the 630 stainless steel shows the $(110)_\alpha$, $(200)_\alpha$, $(211)_\alpha$, and $(220)_\alpha$ peaks of martensite. The patterns for the 316L stainless steel with and without pigment both show the $(111)_\gamma$, $(200)_\gamma$, $(220)_\gamma$, $(311)_\gamma$, and $(222)_\gamma$ peaks of austenite. The intensities of the $(111)_\gamma$, $(200)_\gamma$, and $(220)_\gamma$ noticeably differ. These XRD analysis results cannot explain the difference in tensile properties of the specimens. In addition, no significant microstructural difference is evident in the 316L stainless steel with or without the addition of pigment. The main reason for the lower elongation of 316L stainless steel is its low sintered density of less than 93% resulting from the addition of pigment.

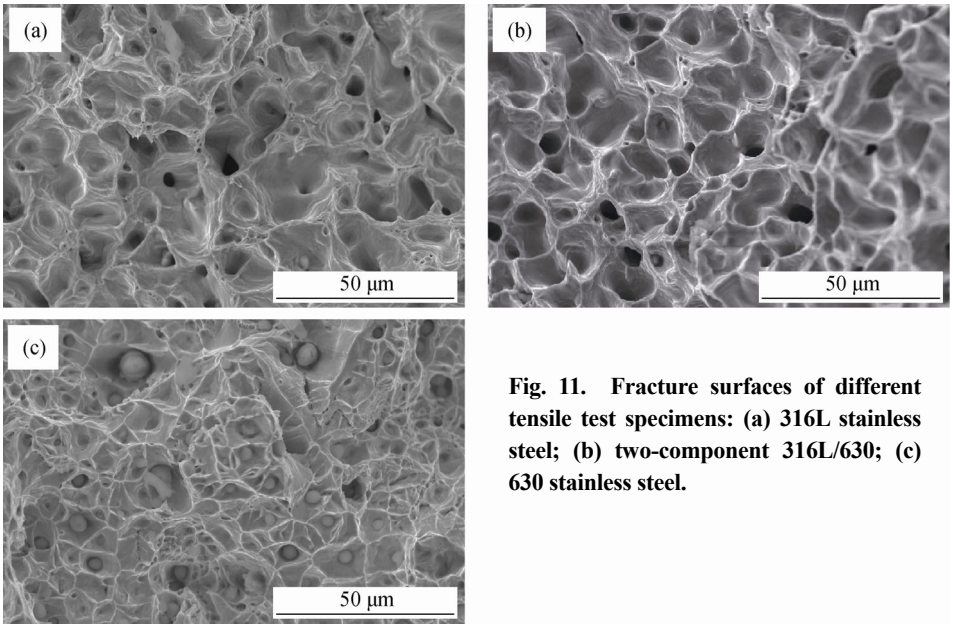

Fig. 11. Fracture surfaces of different tensile test specimens: (a) 316L stainless steel; (b) two-component 316L/630; (c) 630 stainless steel.

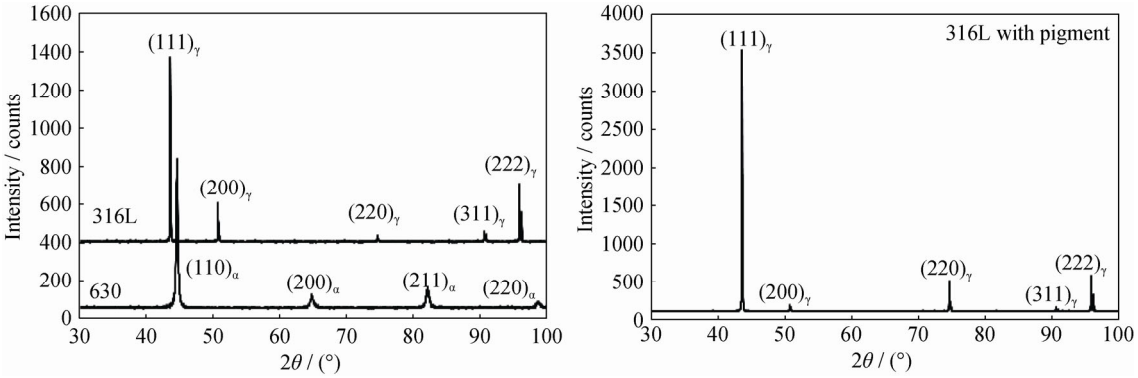

Fig. 12. XRD results for sintered 316L stainless steel, 630 stainless steel, and 316L stainless steel with coloured pigment.

4. Conclusions

Tensile test specimens of mono-component 316L stainless steel, 630 stainless steel, and two-component 316L/630 stainless steel with three different weld line positions were fabricated using a metal-injection moulding process. Pink pigment was added to the 316L stainless steel feedstock at a content of 1.96wt% to enable identification of the weld line and the material. After sintering, both stainless steels exhibited a silver metallic colour with different levels of glossiness. The sintered densities increased with increasing percentage of 630 stainless steel within the gauge length. The linear shrinkages of the two mono-component specimens were lower than those of the two-component specimens because the incompatibility of sintering shrinkage of both materials caused biaxial stresses and enhanced sintering. The

addition of coloured pigment reduced the relative density of 316L to less than 93%. As a result, the mechanical properties of the 316L stainless steel in both the mono-component specimens and the two-component specimens were substantially reduced compared with the typical mechanical properties of 316L. The yield stress and ultimate tensile strength of the two-component specimens were similar to those of the weaker material (316L stainless steel). The fracture always occurred near the interface of the two materials but always on the 316L stainless steel portion. The elongation to failure of the two-component specimens was lower than that of both of the mono-component specimens. For the two-component specimens, the elongation decreased with increasing percentage of 630 stainless steel within the gauge length. On the basis of SEM observation, the microstructures were divided into three zones: one zone for each of the individual materials and an interfacial zone. The width of the interfacial zone was 180 μm. Over this interfacial zone, nickel gradually diffused from the 316L stainless steel toward the 630 stainless steel and copper diffused from the 630 stainless steel toward the 316L stainless steel. The fracture surfaces of the two-material specimens were similar to that of 316L stainless steel.

Acknowledgements

This study was co-funded by the National Metal and Materials Technology Center (MTEC), Thailand and Taisei Kogyo (Thailand) Co., Ltd. (grant number P1451042). The authors declare that they have no conflict of interest. The authors would also like to thank B. Thumrongthayaluk for sample preparation.

References

[1] D.F. Heaney, P. Suri, and R.M. German, Defect-free sintering of two material powder injection molded components. Part I Experimental investigations, *J. Mater. Sci.*, 38(2003), No. 24, p. 4869.

[2] J.R. Alcock, P.M. Logan, and D.J. Stephenson, Surface engineering by co-injection moulding, *Surf. Coat. Technol.*, 105(1998), No. 1-2, p. 65.

[3] P. Imgrund, A. Rota, F. Petzoldt, and A. Simchi, Manufacturing of multi-functional micro parts by two-component metal injection moulding, *Int. J. Adv. Manuf. Technol*., 33(2007), No. 1-2, p. 176.

[4] J.L. Johnson, L.K. Tan, R. Bollina, and R.M. German, Evaluation of copper powders for processing heat sinks by metal injection moulding, *Powder Metall.*, 48(2005), No. 2, p. 123.

[5] P. Suri, Chapter 14 – Two-material/two-color powder metal injection molding (C2-PIM), [in] *Handbook of Metal Injection Moulding*, Edited by Donald Heaney, Woodhead Publishing Limited, Oxford, 2012, p. 338.

[6] J.L. Johnson, L.K. Tan, P. Suri, and R.M. German, Design guidelines for processing bi-material components via powder-injection molding, *JOM*, 55(2003), No. 10, p. 30.

[7] A. Simchi, A. Rota, and P. Imgrund, An investigation on the sintering behavior of 316L and 17-4PH stainless steel powders for graded composites, *Mater. Sci. Eng. A*, 424(2006), No. 1-2, p. 282.

[8] M. Mulser, G. Veltl, and F. Petzoldt, Development of magnetic/non-magnetic stainless steel parts produced by two-component metal injection molding, *Int. J. Precis. Eng. Manuf.*, 17 (2016), No. 3, p. 347.

[9] T. Harikou, Y. Itoh, K. Satoh, and H. Miura, Joining of SUS316L and SUS430L by insert injection molding, *J. Jpn. Soc. Powder Powder Metall.*, 49(2002), No. 9, p. 841.

[10] A. Islam, H. Hansen, M. Marhöfer, J. Angel, B. Dormann, and M. Bondo, Two-component micro injection moulding for hearing aid applications, *Int. J. Adv. Manuf. Technol*., 62(2012), No. 5-8, p. 605.

[11] V. Piotter, N. Holstein, K. Plewa, R.R. Ruprecht, and J. Hausselt, Replication of micro components by different variants of injection molding, *Microsyst. Technol*., 10(2004), No. 6-7, p. 547.

[12] MPIF standard 35: *Materials Standard for Metal Injection Molded Parts*, Metal Powder Industries Federation (MPIF), Princeton, NJ, 2016.

[13] MPIF Standard 42: *Determination of Density of Compacted or Sintered Metal Powder Products*, Metal Powder Industries Federation (MPIF), Princeton, NJ, 2000.

[14] V. Firouzdor, A. Simchi, and A.H. Kokabi, An investigation of the densification and microstructural evolution of M2/316L stepwise graded composite during co-sintering, *J. Mater. Sci.*, 43 (2008), No. 1, p. 55.

[15] V. Firouzdor and A. Simchi, Co-sintering of M2/17-4PH powders for fabrication of functional graded composite layers, *J. Compos. Mater.*, 44 (2010), No. 4, p. 417.

[16] D. Ravi and D.J. Green, Sintering stresses and distortion produced by density differences in bi-layer structures, *J. Eur. Ceram. Soc*., 26(2006), No. 1-2, p. 17.

[17] P. Suri, D.F. Heaney, and R.M. German, Defect-free sintering of two material powder injection molded components. Part II Model, *J. Mater. Sci.*, 38(2003), No. 24, p. 4875.

[18] P. Imgrund, A. Rota, and A. Simchi, Microinjection moulding of 316L/17–4PH and 316L/Fe powders for fabrication of magnetic-nonmagnetic bimetals, *J. Mater. Process. Technol*., 200(2008), No. 1-3, p. 259.

[19] Y.M. Li, L.J. Li, and K.A. Khalil, Effect of powder loading on metal injection molding stainless steels, *J. Mater. Process. Technol*., 183(2007), No. 2-3, p. 432.